Published in final edited form as:

Cancer Res. 2016 August 15; 76(16): 4805–4815. doi:10.1158/0008-5472.CAN-15-2323.

Novel anticancer agents based on targeting the trimer interface of the PRL phosphatase

Yunpeng Bai[1], **Zhi-Hong Yu**[1], **Sijiu Liu**[2], **Lujuan Zhang**[2], **Ruo-Yu Zhang**[1], **Li-Fan Zeng**[2], **Sheng Zhang**[1], and **Zhong-Yin Zhang**[1,2]

Zhong-Yin Zhang: zhang-zy@purdue.edu

[1]Department of Medicinal Chemistry and Molecular Pharmacology, Department of Chemistry, Purdue Center for Cancer Research, and Purdue Center for Drug Discovery, Purdue University, 575 Stadium Mall Drive, West Lafayette, IN 47907, USA

[2]Department of Biochemistry and Molecular Biology, Indiana University School of Medicine, 635 Barnhill Drive, Indianapolis, IN 46202, USA

Abstract

PRL oncoproteins are phosphatases overexpressed in numerous types of human cancer. Elevated levels of PRL associate with metastasis and poor clinical outcomes. In principle, PRL phosphatases offer appealing therapeutic targets, but they remain underexplored due to the lack of specific chemical probes. In this study, we address this issue by exploiting a unique property of PRL phosphatases, namely, that they may function as homotrimers. Starting from a sequential structure-based virtual screening and medicinal chemistry strategy, we identified Cmpd-43 and several analogs which disrupt PRL1 trimerization. Biochemical and structural analyses demonstrate that Cmpd-43 and its close analogs directly bind the PRL1 trimer interface and obstruct PRL1 trimerization. Cmpd-43 also specifically blocks the PRL1-induced cell proliferation and migration through attenuation of both ERK1/2 and Akt activity. Importantly, Cmpd-43 exerted potent anticancer activity both in vitro and in vivo in a murine xenograft model of melanoma. Our results validate a trimerization-dependent signaling mechanism for PRL and offer proof-of-concept for trimerization inhibitors as candidate therapeutics to treat PRL-driven cancers

Introduction

Reversible and coordinated protein tyrosine phosphorylation is central to diverse signal pathways regulating cell growth, migration and survival. Disturbance of the normal pattern of tyrosine phosphorylation, due to perturbed balance between the activities of protein tyrosine kinases (PTKs) and protein tyrosine phosphatases (PTPs), causes abnormal cell

Correspondence to: Zhong-Yin Zhang, zhang-zy@purdue.edu.

Conflict of interest: The authors have no conflicts to disclose.

Data deposition: The coordinates for the structure of the PRL1•Analog-3 complex (accession number 5BX1) have been deposited in the Protein Data Bank.

Supporting Information: *In vitro* and *in vivo* cross-linking experiments, synthesis of Cmpd-43 and its analogs, assessment of PTP inhibition by Cmpd-43, PRL1 expression, purification, crystallization and data collection, structural determination and refinement, histological studies, and supplemental figures S1-S6.

signaling and has been linked to the etiology of many human diseases including cancer (1). Thus there is vast interest in targeting dysfunctional pathways driven by aberrant tyrosine phosphorylation for therapeutic interventions. Notable success has been achieved by targeting the PTKs, as shown by the more than two-dozen small molecule inhibitors already in the clinic (2). However, resistance to kinase inhibitor treatments prevents durable responses. Therefore, there is heightened interest to modulate disease progression at the level of PTPs.

The PRL (phosphatase of regenerating liver) phosphatases constitute a unique group of PTPs, with three closely related members (PRL1, 2 and 3) (3-6). Unlike other PTPs, the PRLs function as positive signal transducers capable of activating both ERK1/2 (7-11) and Akt (12-15), two of the major pathways that are aberrantly up-regulated in cancer (16, 17). PRL1 was initially identified as an immediate early gene induced during liver regeneration upon partial hepatectomy (18). Subsequent studies found that exogenous expression of PRLs accelerates cell proliferation and anchorage-independent growth (7, 18-21). Constitutive PRL expression also promotes cell migration and invasion (7, 8, 11, 22-25). Moreover, PRL overexpressing cells form tumors with high metastatic potential when injected into mice (9, 22, 23, 26), whereas PRL knockdown reduces cell proliferation and migration as well as tumorigenesis *in vivo* (9, 11, 25, 27-30) Most significantly, PRL level is elevated in human cancers of colon (31, 32), liver (23, 33), ovarian (27, 34), prostate (35), gastric (36, 37), pancreatic (13), and breast (9, 38), as well as in melanoma (20, 39), multiple myeloma (40) and acute myeloid leukemia (41, 42), and PRL overexpression strongly correlates with late stage metastasis and poor clinical outcomes. Taken together, the data implicate PRLs as novel molecular markers and therapeutic targets for metastatic cancers. Consequently, PRLs have garnered considerable interest for drug discovery (6). Unfortunately, the rather flat PRL active site and its structural similarity to other members of the PTP family present significant challenge for PRL inhibitor design. Indeed, reported active site directed PRL inhibitors are neither sufficiently potent nor selective, and so are not suitable for *in vivo* pharmacological study and therapeutic development (6).

We describe a novel approach to inhibit PRL function by targeting a unique structural and regulatory property of the PRLs. One of the most striking features of PRL1 is that it exists as a trimer in the crystalline state and has a high propensity to form trimer in solution and inside the cell (8, 10, 43, 44). Moreover, trimer formation is essential for PRL1-mediated cell growth and migration, suggesting that small molecules targeting the trimeric interface of PRLs could potentially have therapeutic value (8). To capitalize on these findings, we used a computer-based virtual screen to search the available chemical databases for compounds capable of disrupting PRL trimerization. Biochemical and structural analyses demonstrate that Cmpd-43 and its close analogs bind the PRL1 trimer interface and block PRL1 trimerization. Cmpd-43 also specifically abrogates the PRL1-induced cell proliferation and migration through attenuation of both ERK1/2 and Akt activity. Importantly, Cmpd-43 exhibits excellent anti-cancer activity both *in vitro* and in a xenograft mouse model of melanoma. The study provides pharmacological validation that trimerization is important for PRL1 function and targeting PRL trimerization is a viable approach for therapeutic development.

Materials and Methods

Materials

Anti-HA, anti-tubulin and anti-GAPDH antibodies were purchased from Santa Cruz Biotechnology. Anti-ERK1/2, anti-pERK1/2 (Thr202/Tyr204), anti-Akt, anti-pAkt (Ser473) and anti-LSD1 antibodies were obtained from Cell Signaling. Dulbecco's modified Eagle's medium (DMEM), fetal bovine serum, penicillin, and streptomycin were from Invitrogen. HEK293, MeWo and MCF7 cell lines were purchased directly from ATCC between 2008 and 2015. The ATCC cell lines were characterized by short tandem repeat (STR) DNA profiling. MCF10A cell was received as a gift from Dr. Mircea Ivan's lab in Indiana University School of Medicine, and was authenticated by morphology. All cell lines were passaged for fewer than 6 months after resuscitation.

Virtual screening

Asinex and ChemBridge subsets in ZINC (45) database were downloaded from ZINC website (http://zinc.docking.org) and used for virtual screening. The monomer B in PRL1 trimer structure (PDBID: 1ZCK) (44) was used as receptor, and the coordinates were retrieved from the Protein Data Bank. The *DOCK6.2* program (46) was used for rigid docking to generate a potential subset of molecules binding at PRL1 trimer interface, and then AutoDock4.01 software (47) was used for flexible docking to get the most potent hits.

In the first stage docking, the structure of monomer B was processed using the “Dock Prep” module in UCSF CHIMERA, then the docking region was defined through a standard pipeline of running *dms*, *sphgen, sphere_selector* and *showbox* program, and the energy scoring values were calculated by *grid* program. About 560,000 small molecules (downloaded in 28 mol2 files, ~20,000 molecules in each file) were submitted to the *dock6.mpi* program to perform docking calculations simultaneously. During each docking, the small molecule was positioned with 1,000 orientations, the lowest interaction energy and corresponding conformation was recorded. All ligands in each mol2 file were ranked according to their lowest interaction energy, and the top 2,000 were kept for the second stage docking, thus 56,000 (2,000 × 28) molecules were picked out for next stage screening.

In the second stage docking, the structure of monomer B was processed in AutoDockTools1.4 software, Gasteiger charge was added and non-polar hydrogens were merged. The docking area was designated around the BA- or BC-interface, and the energy grids of 51 × 51 × 73 points with 0.375 Å spacing on each axis were calculated for 17 atom types (H, HD, HS, C, A, N, NA, NS, OA, OS, F, P, SA, S, Cl, Br and I), as well as the electrostatic and desolvation potential using *autogrid4* program; On the other hand, each ligand structure was used to generate pdbqt and dpf files using *prepare_ligand4.py* and *prepare_dpf4.py* scripts. Based on these prepared files, molecular docking was carried out in *autodock4* program as follows: 10 separate docking runs were performed for each ligand. In each docking run, the optimal binding conformation was achieved by Lamarckian Genetic Algorithm with Local Search (LGALS) method. After all ligands were docked, the lowest binding free energy of each ligand was extracted and ranked, and hit molecules were picked

out through binding free energy comparisons, structure similarity analyses and binding mode inspections.

Cell culture and transfection

HEK293, MeWo, and MCF7 cells were grown in DMEM supplemented with 10% fetal bovine serum, penicillin (50 units/mL), and streptomycin (50 μg/mL) in a 37°C incubator containing 5% CO_2. MCF10A cells were grown in MEBM medium supplemented with MEGM Single Quots and 100 ng/mL cholera toxin (Lonza, Basel, Switzerland). HEK293 cells were seeded at 40% confluence in antibiotic-free medium and grown overnight. Transfection was performed using Lipofectamine 2000 from Invitrogen according to the manufacturer's recommendations.

Wound healing assay

Cells were grown to 90% confluence in a 12-well plate at 37 °C in an atmosphere of 5% CO_2. A wound was created by scratching cells with a sterile 200 μL pipette tip. Cells were washed with PBS to remove the floating cells, and then treated with fresh medium containing 20 μM compound or DMSO. The wounds were photographed at 0 hour and 24 hours under ×10 magnitude microscope. Wound healing magnitude was quantified by measuring the relative wound closure compared with control cells at 24 hours.

MTT assay

Cells were seeded in a 96-multiwell plate (3000 cells/well) containing DMEM, 10% fetal bovine serum at 37 °C in an atmosphere of 5% CO_2 overnight. Cells were then treated with various concentrations of compounds or DMSO for 24 and 48 hours. Cell proliferation was then determined by MTT assay as described previously (8) using a multiwall spectrophotometer. Data are presented as relative proliferation rate compared with control cells.

Cell migration assay

Cell migration was determined as described previously (10) with some modifications. The assay was performed with Transwells (6.5 mm diameter; 8 μM pore size polycarbonate membrane) obtained from Corning (Costar, Acton, MA). Cells (3.75×10^5) in 1.5 mL of serum-free medium were placed in the upper chamber, whereas the lower chamber was loaded with 2.5 mL of medium containing 10% FBS. Cells were then treated with 10 μM of different compounds as indicated. After 24 hour incubation (37 °C, 5% CO_2), the total number of cells that had migrated into the lower chamber was counted with a hemacytometer. Data are presented as relative migration rate compared with control cells. Cell motility of MeWo cells was also measured using live-cell imaging. 5×10^3/well of MeWo cells were seeded in a 96-well plate for overnight and then treated with 5 μM of Cmpd-43 for 4 hours. 1μg/mL of Hoechst 33342 was used to label the nuclei, and Thermo Scientific ArrayScan XTI Live High Content Platform was then used for live-cell tracking to measure the motility in the presence of Cmpd-43. Motility of the cells was assessed over 6 h and image data were collected every 30 min.

Animal experiments

NSG (NOD/scid/IL2Rg^{null}) mice were purchased from In Vivo Therapeutics Core at Indiana University Simon Cancer Center. Experiments on mice were carried out in accordance with the regulations of The Institutional Animal Care and Use Committees at Indiana University. All mice were housed under pathogen-free conditions in the animal facility and received autoclaved water and food. 10-12 weeks old NSG mice were used in the study. MeWo cells were suspended in phosphate-buffered saline (PBS) at 8×10^7 cells/ml. A total of 8×10^6 cells (100 μl) were subcutaneously implanted into both left and right flank (n=24) using a 27-gauge needle. Once the tumor volume reaches 200 mm^3, daily intraperitoneal injection of either control or 30 mg/kg Cmpd-43 was performed, and the tumor growth was monitored for 3 weeks. Tumor volume was calculated using the formula $V=(W^2\times L)/2$ for caliper measurements. Mice were sacrificed after injection for 21 days, and organs were collected for immunohistological and biochemical analysis.

Statistics

For cell-based proliferation, migration and wound healing assays, the Student's t test was used to measure the significance. For MeWo cell xenograft tumors, tumor volumes at different time and final tumor weights were compared using the Student's t test. In comparing the mRNA level of PRLs in human normal skin and melanoma samples, Student's t test was used assess the significance of differences between groups. Survival analysis was performed according to the Kaplan-Meier method and the log-rank test, a p-value of less than 0.05 was considered statistically significant.

Results and Discussion

Identification of small molecule PRL1 detrimerizers

Given the functional requirement of PRL trimerization, disruption of PRL trimerization was proposed as a potential therapeutic approach for PRL-based drug discovery (8), but this strategy has not been validated with pharmacologic approaches. As revealed by the homotrimeric PRL1 crystal structure (44), each PRL1 monomer (e.g. monomer B) has two dimer interfaces, namely the BA- (residues from 125 to 150) and BC-interfaces (residues from 11 to 18, 36 to 41, and 92 to 98), which are 18 and 19 Å away from the active site Cys104 in the catalytic P-loop C_{104}VAGLGR$_{110}$ (Figure 1A). To discover small molecules capable of blocking PRL1 trimerization, we used structure-based virtual screening to identify compounds that bind to the dimer interfaces in each PRL1 monomer. We employed a sequential screening strategy, starting with rigid docking in DOCK6.2 (46) to sample a total of 560,000 compounds (Asinex and ChemBridge subsets in the ZINC database) (45) to each dimer interface and score protein–ligand complexes based on the calculated interaction energies, which was followed by flexible docking in AutoDock4.01 (47) to analyze the top 10% hits obtained from rigid docking (Figure 1B). This process led to the selection of 100 top-ranked compounds for each interface. Upon further binding mode verification and structural similarity analyses, 56 structurally diverse compounds were purchased for further experimental evaluation.

The ability of the 56 compounds to disrupt PRL1 trimerization was initially assessed by *in vitro* cross-linking experiments using recombinant PRL1 protein (44). Ten out of the 56 compounds exhibited significant activity in blocking PRL1 trimerization. To further confirm the efficiency of these compounds to disrupt PRL1 trimer formation, we also evaluated them in an *in vivo* cell-based cross-linking assay. HA-tagged PRL1 expressing HEK293 cells were treated with the compounds, fixed with 1% formaldehyde, and the HA-tagged PRL1 was immunoprecipitated with HA antibodies, analyzed by SDS-PAGE and visualized by immunoblotting with anti-HA antibodies. As shown in Figure 1C, the top three compounds, Cmpd-3, Cmpd-26 and Cmpd-43, significantly decreased PRL1 trimer formation inside the cell, with Cmpd-43 being the most potent PRL1 detrimerizer (Figure 1D). Importantly, Cmpd-43 at 20 μM did not inhibit the phosphatase activity of PRL1 as well as a large panel of PTPs including receptor-like PTPs, PTPμ, PTPε, LAR, PTPσ and PTPγ, cytosolic PTPs, PTP1B, Lyp, SHP1, PTPH1, HePTP, STEP, and PEZ, the dual specificity phosphatase VHR, VHZ, MKP5, CDC14A, and the low molecular weight PTP.

Given that PRL1 trimerization is essential for the PRL1 mediated cell proliferation and migration (8), Cmpd-43 is expected to suppress both cellular processes if it disrupts PRL1 trimerization inside the cell. To test this hypothesis, we determined the effect of Cmpd-43 on cell proliferation and migration in PRL1 expressing HEK293 cells. As expected, Cmpd-43 inhibited PRL1 induced cell proliferation in a dose dependent manner (Figure 1E). In addition, Cmpd-43 also markedly delayed the wound closure induced by PRL1 overexpression (Figure 1F). To delineate the structural features of Cmpd-43 important for inhibiting PRL1 mediated cellular processes, a series of Cmpd-43 derivatives were either purchased (Analogs 1 to 4) or synthesized (Analogs 5 to 7) (Figure 2A). As shown in Figure 2B&C, Analog-3 displayed similar efficacy as Cmpd-43 in attenuating PRL1 induced cell proliferation and migration, while Analogs 2 and 4-7 appeared slightly less effective than Cmpd-43. Interestingly, Analog-1 exerted no effect on either cell proliferation or migration, suggesting that the iminomethyl-aromatic moiety, which is missing in Analog-1, is critical for the inhibitory activity of Cmpd-43 and the other 6 analogs. Collectively, through a two-stage virtual screening strategy, biochemical and cell based evaluation, and a limited structure and activity analysis, we identified Cmpd-43 and several analogs as potential disruptors of PRL1 trimerization. We also found a structurally related but inactive Analog 1, which could serve as a negative control in mechanistic studies.

Cmpd-43 specifically blocks PRL1 mediated signaling, cell proliferation and migration

Before Cmpd-43 can be used as a chemical probe to address PRL1's roles in normal physiology and in cancer and serve as a lead for therapeutic development, it is important to establish whether Cmpd-43 exerts its effect inside the cell through disruption of PRL1 trimerization and inhibition of PRL1-mediated signaling. To this end, we first compared the effect of Cmpd-43 and its inactive Analog-1 on PRL1 trimerization. As shown in Figure 3A, Cmpd-43 effectively blocked PRL1 trimerization in HEK293 cells while at the same concentration Analog-1 had no effect, consistent with its lack of inhibition in PRL1 mediated cell proliferation and migration (Figure 2B&C). To further evaluate the specificity of Cmpd-43, we utilized a trimerization deficient mutant PRL1/G97R, which is incapable of promoting cell growth and migration (8). Thus Cmpd-43 would not be expected to affect the

growth and migration of PRL1/G97R expressing cells if its main mode of action is disrupting PRL1 trimerization. We first confirmed that PRL1/G97R was defective in trimer formation (Figure 3B). We also confirmed that while ectopic expression of PRL1 increased both cell proliferation and migration, the rates for the PRL1/G97R cells were similar to those of the vector control cells (Figure 3C&D), again validating the functional importance of PRL1 trimerization. We then measured the effect of Cmpd-43 and Analog-1 on the proliferation and migration of both wild-type PRL1 and PRL1/G97R expressing cells. As expected, treatment with Cmpd-43, but not Analog-1, attenuated PRL1-induced cell proliferation in a dose-dependent manner, while neither Analog-1 nor Cmpd-43 had any effect on PRL1/G97R expressing cell proliferation (Figure 3C). Similarly, Cmpd-43, but not Analog-1, was capable of reducing wild-type PRL1 induced cell migration, whereas neither Cmpd-43 nor Analog-1 was able to alter the cell migration behavior of the PRL1/G97R expressing cells (Figure 3D). Finally, we evaluated Cmpd-43 in mouse embryo fibroblast (MEF) derived from either wild-type or PRL1 deficient mice. As expected, Cmpd-43 preferentially inhibited wild-type over $PRL1^{-/-}$ MEF cells (Supplemental Figure 1), indicating that Cmpd-43 exerted its anti-proliferative activity through blocking PRL1 trimerization.

PRL1 promotes cell proliferation and migration through activation of ERK1/2 and Akt pathways (8, 13, 24). To delineate the biochemical mechanism by which Cmpd-43 exerts its inhibitory activity on cell growth and migration, we analyzed the effect of Cmpd-43 and Analog-1 on ERK1/2 and Akt activity in both wild-type PRL1 and the trimerization impaired PRL1/G97R mutant expressing cells. Consistent with the results from the phenotypic assays, expression of PRL1 increased ERK1/2 and Akt activity by 3.4 and 2.5-fold, respectively, whereas the activation status of ERK1/2 and Akt in PRL1/G97R cells was similar to that of the vector control cells (Figure 3E). As expected, Cmpd-43 effectively abrogated the PRL1-induced ERK1/2 and Akt activation whereas the negative control Analog-1 had no effect on ERK/1/2 and Akt activity. In line with PRL1/G97R being a loss of function mutant, neither Cmpd-43 nor Analog-1 had any effect on ERK1/2 and Akt signaling in PRL1/G97R cells. Collectively, these mechanistic studies provide additional strong evidence that Cmpd-43 inhibits PRL1-mediated cellular signaling as well as cell proliferation and migration by blocking PRL1 trimerization.

Analog-3 binds to the PRL1 trimer interfaces and blocks PRL1 trimerization

To provide direct evidence that Cmpd-43 binds to the PRL1 trimer interfaces and to determine the molecular basis of PRL1 detrimerization by Cmpd-43, we sought to co-crystallize PRL1 with Cmpd-43 as well as Analog-3. We obtained co-crystals of PRL1 bound with Analog-3. The 3D structure of PRL1•Analog-3 complex was solved by molecular replacement using monomer A in the PRL1 trimer structure (PDBID: 1ZCK) (44) as a search model and refined to 1.90 Å resolution. The final atomic model encompasses residues 4-160 of PRL1 and the intact Analog-3, which is unambiguously identified by the unbiased F_o-F_c omit density map (Figure 4A). The details of data collection and structure refinement are summarized in Table 1. The complex structure belongs to the $C222_1$ space group with one PRL1 molecule per asymmetric unit. Remarkably, while a homotrimeric arrangement was always observed in previous crystal structures of wild-type PRL1 (43, 44),

the PRL1/C104S mutant in complex with sulfate in the active site (44), and PRL1 in complex with a peptide ligand (10), the PRL1•Analog-3 complex crystallized as a monomer. The overall structure of PRL1•Analog-3 is quite similar to the initial search model used for molecular replacement. PRL1 adopts a compact α+β structure comprising a central five-stranded β sheet surrounded by four α helixes on one side and two α helixes on the other side (Figure 4A). The PTP signature motif (C_{104}VAGLGR$_{110}$) forms a loop (P-loop) between β5 and α4 located at the base of the active site pocket. The binding site for Analog-3 is situated at the backside of the PRL1 active site, which is defined by residues within the α5 helix, α4-α5 loop, β1-β2 hairpin and the C-terminus (Figure 4A). Interestingly, residues involved in binding Analog-3 come from both the BC- and BA-dimer interfaces in the resolved complex crystal structure, with the majority of the contact area in the BC-interface (Figure 4B).

Figure 4C shows the detailed interactions between PRL1 and Analog-3. The dimethyl-isoindoline moiety is placed within a hydrophobic pocket defined by Tyr14, Met124, Phe132 and the aliphatic carbon atoms in Asp128. Specifically, the two methyl groups interact with Asp128 and Phe132 respectively, while the isoindoline moiety makes contacts with Tyr14, Met124 and Phe132. The adjacent benzohydrazide motif has several van der Waals contacts with residues Thr13, Tyr14 and Lys15, and the oxygen atom provides an additional polar interaction with terminal amine of Lys15. The furan ring extends into a cavity constituted by Lys15, Asn16 and Arg159, making van der Waals interactions with these residues as well as a polar interaction between the oxygen atom and the side chain of Asn16.

To further substantiate the molecular interactions between PRL1 and Analog-3, we mutated Tyr14 and Phe132, which have strong hydrophobic contacts with Analog-3 (Figure 4C). Analyses of the buried surface area in the dimer interfaces indicated that these two residues make very limited, if any, contribution to PRL1 trimerization. Thus we predicated that substitutions at Tyr14 and Phe132 would weaken the interaction between PRL1 and Analog-3/Cmpd-43, without interference with PRL1 trimerization. As expected, replacement of Tyr14 and Phe132 by an Ala had no effect on PRL1 trimerization and PRL1-mediated cell migration (Figure 4D&E). Importantly, the PRL1/Y14A and PRL1/F132A mutants were resistant to Cmpd-43 treatment. Indeed, while Cmpd-43 blocked wild-type PRL1 trimerization as well as PRL1-mediated cell migration, it failed to inhibit PRL1/Y14A and PRL1/F132A trimer formation and had little effect on PRL1/Y14A or PRL1/F132A mediated cell migration (Figure 4D&E). These results are in complete agreement with the structural observations that residues Tyr14 and Phe132 are involved in binding Analog-3. Taken together, the structural and mutagenesis data provide direct evidence that Analog-3 and Cmpd-43 bind at the PRL1 trimer interface and prevents PRL1 trimerization.

PRL1 detrimerizer Cmpd-43 exhibits anti-cancer activity

As mentioned in the introduction, PRLs are overexpressed in many tumor cell lines. To investigate the clinical relevance of PRL overexpression and tumor progression, we analyzed the Gene Expression across Normal and Tumor tissue (GENT) database, a publicly available microarray dataset containing more than 34,000 human cancer and normal samples (48). We found that samples from melanoma patients (n=302) had significantly higher PRL1 and

PRL2 mRNA expression compared to normal skin samples (n=141) (Figure 5A&B). To further evaluate the significance of PRL1 overexpression in predicting survival in patients with melanoma, we analyzed The Cancer Genome Atlas (TCGA) skin cutaneous melanoma dataset. Consistent with the oncogenic role of PRL1 in human melanoma samples, patients with high PRL1 mRNA expression had significantly decreased survival (n=53, median survival=72.8 months) compared with those with low PRL1 mRNA expression in the melanoma (n=57, median survival=362.3 months), with a hazard ratio (HR) of 0.46 (95% CI of ratio=0.24 to 0.88, p=0.019) (Figure 5C). These clinical data suggest that inhibition of PRL1 could be beneficial for melanoma treatment. Thus we hypothesized that the PRL1 detrimerizer Cmpd-43 may exhibit anti-melanoma activity, possibly via downregulating the activity of both ERK1/2 and Akt pathways. To directly test this hypothesis, we examined whether Cmpd-43 could suppress human melanoma MeWo cell growth and motility. As shown in Figure 5D, Cmpd-43 dose-dependently decreased MeWo cell proliferation as measured by the MTT assay. Live-cell tracking was used to measure the motility of MeWo cells in the presence of Cmpd-43. As shown in Figure 5E, the total distance traveled over 6 hours for Cmpd-43 treated MeWo cells was significantly less than that of the control cells. To determine whether Cmpd-43 preferentially inhibits cancer cell growth, we treated both mammary carcinoma cell line MCF7 and normal mammary epithelial cell line MCF10A with Cmpd-43. As observed with MeWo cells, Cmpd-43 dose-dependently suppressed the growth of MCF7 breast cancer cells, but the inhibitory effect of Cmpd-43 was significantly compromised towards non-tumorigenic MCF10A cells (Supplemental Figure 2A). In addition, the anti-proliferative activity of Cmpd-43 to MEF cells was also significantly reduced when compared to the MeWo cells (Supplemental Figure 2B). These data indicate that Cmpd-43 displays significantly lower cell toxicity toward normal cells.

Importantly, Cmpd-43 treatment dose-dependently reduced HGF-induced ERK1/2 and Akt phosphorylation (Figure 5F). To make certain that the effect of Cmpd-43 in MeWo cells is also mediated by blocking PRL1 trimerization, we overexpressed either wild-type PRL1 or the trimerization deficient mutant PRL1/G97R mutant in MeWo cells. Similar to what we observed in HEK293 cells (Figure 3E), we found that overexpression of PRL1 but not PRL1/G97R significantly enhanced both ERK1/2 and Akt phosphorylation by about ~2 fold (Figure 5G). More importantly, Cmpd-43 but not Analog-1 suppressed PRL1-induced ERK1/2 and Akt activation. However, neither Cmpd-43 nor Analog-1 were able to reduce pERK1/2 and pAkt levels in PRL1/G97R expressing MeWo cells (Figure 5G), suggesting that Cmpd-43 inhibits PRL1-induced ERK1/2 and Akt activation in MeWo cells by blocking PRL1 trimerization.

The PRL1 crystal structure revealed that residues at the trimer interface are conserved among all three PRLs (44, Supplemental Figure 3A). We previously showed that like PRL1, PRL3 could also form trimer in solution and inside the cells (8, 44). Amino acid sequence alignment shows that key residues involved in Analog-3 binding are also highly conserved among all three PRLs (Supplemental Figure 3A). Therefore, we hypothesized that trimerization is a general property for all PRLs and Cmpd-43 should inhibit trimerization of all PRLs. Indeed, both PRL2 and PRL3 can form trimer, and Cmpd-43 but not Analog-1 significantly reduces PRL2 and PRL3 trimer formation (Supplemental Figure 3B).

To further validate the specificity of Cmpd-43 for PRLs in MeWo cells, we knocked down both PRL1 and PRL2, which are the major PRL isoforms expressed in MeWo cells. We first demonstrated that knocking down both PRL1 and PRL2 significantly reduced ERK1/2 and Akt activation in MeWo cells (Supplemental Figure 4). In addition, the dose-dependent inhibition of both pERK1/2 and pAkt by Cmpd-43 in scramble siRNA treated MeWo cells was significantly compromised in PRL1 and PRL2 knocked down cells (Figure 5H&I). These data suggest that Cmpd-43 inhibits both ERK1/2 and Akt signaling pathways in MeWo cells specifically through targeting both PRL1 and PRL2. Overall, these results demonstrate that pharmacologic inhibition of PRL trimerization in MeWo cells attenuates both the ERK1/2 and Akt pathway activation and inhibits cell proliferation and motility.

Given the promising activity of Cmpd-43 in cell-based assays, we next aimed to establish the therapeutic potential of targeting PRL with Cmpd-43. First, we characterized the pharmacokinetic properties of Cmpd-43 in mice. Cmpd-43 displayed a very respectable pharmacokinetic profile in mouse with a plasma compound exposure C_{max}=0.3 μM and a half-life $t_{1/2}$=15.8 h at a single 20 mg/kg intraperitoneal dosage. We then assessed the effect of Cmpd-43 on *in vivo* tumor growth in a mouse xenograft model using MeWo cells subcutaneously implanted into immunodeficient NSG mice. Once the tumor volume reached 200 mm^3, we started daily intraperitoneal injection of either vehicle control or 30 mg/kg Cmpd-43 and monitored the tumor growth for 3 weeks. Mice treated with Cmpd-43 displayed reduced tumor growth throughout the experiment compared with mice treated with vehicle control (Figure 6A). At 21 days post treatment, we collected the tumors (Supplemental Figure 5), and observed a ~62% shrinkage in tumor volume and ~48% reduction in tumor weight (Figure 6A&B). Dissection and histological analyses revealed no apparent toxicity in major organs when the mice were treated with Cmpd-43 at 30 mg/kg (Supplemental Figure 6A&B). Furthermore, biochemical studies performed in samples isolated from the melanoma tumors revealed substantial reduction in both ERK1/2 and Akt phosphorylation, upon treatment with Cmpd-43 (Figure 6C). Immunohistological analyses of tumor tissues revealed significantly reduced proliferation and increased apoptosis in Cmpd-43 treated MeWo tumors (Figure 6D). Taken together, the reduction in tumor growth correlated with a decrease in ERK1/2 and Akt activity, validating the on-target activities of Cmpd-43.

In summary, recent studies expose an oncogenic role of PRLs in many cancers (3-6), raising the possibility that inhibition of these phosphatases might have broader therapeutic applications in oncology. Interestingly, the oncogenic potential of PRLs is always associated with their overexpression, which should increase the propensity of PRL trimerization inside the cell. Given the functional requirement of PRL trimerization, pharmacologic disruption of PRL trimerization represents an innovative approach for the treatment of human cancers with elevated PRL expression. By targeting the unique, noncatalytic trimerization interfaces that are unrelated to any other member of the PTP family, such PRL detrimerizers would be highly specific to the PRL. Starting from a sequential structure-based virtual screening strategy, we have identified Cmpd-43 and several analogs that are capable of preventing PRL trimerization. Biochemical and structural analyses demonstrate that Cmpd-43 and its close analogs directly bind the PRL1 trimer interface and obstruct PRL1 trimerization. Cmpd-43 also specifically blocks the PRL-induced cell proliferation and migration through attenuation

of both ERK1/2 and Akt activity. Importantly, Cmpd-43 exhibits excellent anti-cancer activity both *in vitro* and in a xenograft mouse model of melanoma. The results not only further validate the importance of trimerization for PRL function but also support the clinical potential of compounds that inhibit PRL trimerization. Although additional medicinal chemistry optimization is required, these PRL detrimerizers represent valuable tools for elucidating PRL signaling and for developing novel agents for cancer therapy.

Supplementary Material

Refer to Web version on PubMed Central for supplementary material.

Acknowledgments

This work was supported in part by National Institutes of Health Grants CA69202 (Z.-Y. Zhang) and P30CA023168 (T. Ratliff).

References

1. Hunter T. Tyrosine phosphorylation: thirty years and counting. Curr Opin Cell Biol. 2009; 21:140–6. [PubMed: 19269802]
2. Cohen P, Alessi DR. Kinase Drug Discovery - What's Next in the Field? ACS Chem Biol. 2013; 8:96–104. [PubMed: 23276252]
3. Stephens BJ, Han H, Gokhale V, Von Hoff DD. PRL phosphatases as potential molecular targets in cancer. Mol Cancer Therap. 2005; 4:1653–61. [PubMed: 16275986]
4. Bessette DC, Qiu D, Pallen CJ. PRL PTPs: mediators and markers of cancer progression. Cancer Metastasis Rev. 2008; 27:231–52. [PubMed: 18224294]
5. Rios P, Li X, Köhn M. Molecular mechanisms of the PRL phosphatases. FEBS J. 2013; 280:505–24. [PubMed: 22413991]
6. Campbell AM, Zhang ZY. Phosphatase of Regenerating Liver, a Novel Target for Cancer Therapy. Expert Opin Ther Targets. 2014; 18:555–69. [PubMed: 24579927]
7. Liang F, Liang J, Wang WQ, Sun JP, Udho E, Zhang ZY. PRL3 promotes cell invasion and proliferation by down-regulation of Csk leading to Src activation. J Biol Chem. 2007; 282:5413–9. [PubMed: 17192274]
8. Sun JP, Luo Y, Yu X, Wang WQ, Zhou B, Liang F, et al. Phosphatase activity, trimerization, and the C-terminal polybasic region are all required for the PRL1-mediated cell growth and migration. J Biol Chem. 2007; 282:29043–51. [PubMed: 17656357]
9. Hardy S, Wong NN, Muller WJ, Park M, Tremblay ML. Overexpression of the protein tyrosine phosphatase PRL-2 correlates with breast tumor formation and progression. Cancer Research. 2010; 70:8959–67. [PubMed: 20841483]
10. Bai Y, Luo Y, Liu S, Zhang L, Shen K, Dong Y, et al. PRL-1 protein promotes ERK1/2 and RhoA protein activation through a non-canonical interaction with the Src homology 3 domain of p115 Rho GTPase-activating protein. J Biol Chem. 2011; 286:42316–24. [PubMed: 22009749]
11. Wang Y, Lazo JS. Metastasis-associated phosphatase PRL-2 regulates tumor cell migration and invasion. Oncogene. 2012; 31:818–27. [PubMed: 21765462]
12. Wang H, Quah SY, Dong JM, Manser E, Tang JP, Zeng Q. PRL-3 down-regulates PTEN expression and signals through PI3K to promote epithelial-mesenchymal transition. Cancer Res. 2007; 67:2922–6. [PubMed: 17409395]
13. Stephens B, Han H, Hostetter G, Demeure MJ, Von Hoff DD. Small interfering RNA-mediated knockdown of PRL phosphatases results in altered Akt phosphorylation and reduced clonogenicity of pancreatic cancer cells. Mol Cancer Ther. 2008; 7:202–10. [PubMed: 18187808]

14. Dong Y, Zhang L, Zhang S, Bai Y, Chen H, Sun X, et al. Phosphatase of regenerating liver 2 (PRL2) is essential for placental development by down-regulating PTEN and activating Akt protein. J Biol Chem. 2012; 287:32172–9. [PubMed: 22791713]
15. Dong Y, Zhang L, Bai Y, Zhou HM, Campbell AM, Chen H, et al. Phosphatase of regenerating liver 2 (PRL2) deficiency impairs Kit signaling and spermatogenesis. J Biol Chem. 2014; 289:3799–810. [PubMed: 24371141]
16. Dhillon AS, Hagan S, Rath O, Kolch W. MAP kinase signalling pathways in cancer. Oncogene. 2007; 26:3279–90. [PubMed: 17496922]
17. Vivanco I, Sawyers CL. The phosphatidylinositol 3-Kinase AKT pathway in human cancer. Nature Reviews Cancer. 2002; 2:489–501. [PubMed: 12094235]
18. Diamond RH, Cressman DE, Laz TM, Abrams CS, Taub R. PRL-1, a unique nuclear protein tyrosine phosphatase, affects cell growth. Mol Cell Biol. 1994; 14:3752–62. [PubMed: 8196618]
19. Cates CA, Michael RL, Stayrook KR, Harvey KA, Burke YD, Randall SK, et al. Prenylation of oncogenic human PTP protein tyrosine phosphatases. Cancer Lett. 1996; 110:49–55. [PubMed: 9018080]
20. Wang J, Kirby CE, Herbst R. The tyrosine phosphatase PRL-1 localizes to the endoplasmic reticulum and the mitotic spindle and is required for normal mitosis. J Biol Chem. 2002; 277:46659–68. [PubMed: 12235145]
21. Werner SR, Lee PA, DeCamp MW, Crowell DN, Randall SK, Crowell PL. Enhanced cell cycle progression and down regulation of p21(Cip1/Waf1) by PRL tyrosine phosphatases. Cancer Lett. 2003; 202:201–11. [PubMed: 14643450]
22. Zeng Q, Dong JM, Guo K, Li J, Tan HX, Koh V, et al. PRL-3 and PRL-1 promote cell migration, invasion, and metastasis. Cancer Res. 2003; 63:2716–22. [PubMed: 12782572]
23. Wu X, Zeng H, Zhang X, Zhao Y, Sha H, Ge X, et al. Phosphatase of regenerating liver-3 promotes motility and metastasis of mouse melanoma cells. Am J Pathol. 2004; 164:2039–54. [PubMed: 15161639]
24. Fiordalisi JJ, Keller PJ, Cox AD. PRL tyrosine phosphatases regulate rho family GTPases to promote invasion and motility. Cancer Res. 2006; 66:3153–61. [PubMed: 16540666]
25. Achiwa H, Lazo JS. PRL-1 tyrosine phosphatase regulates c-Src levels, adherence, and invasion in human lung cancer cells. Cancer Res. 2007; 67:643–50. [PubMed: 17234774]
26. Guo K, Li J, Tang JP, Koh V, Gan BQ, Zeng Q. Catalytic domain of PRL-3 plays an essential role in tumor metastasis: formation of PRL-3 tumors inside the blood vessels. Cancer Biol Ther. 2004; 3:945–51. [PubMed: 15326366]
27. Polato F, Codegoni A, Fruscio R, Perego P, Mangioni C, Saha S, et al. PRL-3 phosphatase is implicated in ovarian cancer growth. Clin Cancer Res. 2005; 11:6835–9. [PubMed: 16203771]
28. Kato H, Semba S, Miskad UA, Seo Y, Kasuga M, Yokozaki H. High expression of PRL-3 promotes cancer cell motility and liver metastasis in human colorectal cancer: a predictive molecular marker of metachronous liver and lung metastases. Clin Cancer Res. 2004; 10:7318–28. [PubMed: 15534108]
29. Li Z, Zhan W, Wang Z, Zhu B, He Y, Peng J, et al. Inhibition of PRL-3 gene expression in gastric cancer cell line SGC7901 via microRNA suppressed reduces peritoneal metastasis. Biochem Biophys Res Commun. 2006; 348:229–37. [PubMed: 16875667]
30. Qian F, Li YP, Sheng X, Zhang ZC, Song R, Dong W, et al. PRL-3 siRNA inhibits the metastasis of B16-BL6 mouse melanoma cells in vitro and in vivo. Mol Med. 2007; 13:151–159. [PubMed: 17592549]
31. Saha S, Bardelli A, Buckhaults P, Velculescu VE, Rago C, St Croix B, et al. A phosphatase associated with metastasis of colorectal cancer. Science. 2001; 294:1343–6. [PubMed: 11598267]
32. Peng L, Ning J, Meng L, Shou C. The association of the expression level of protein tyrosine phosphatase PRL-3 protein with liver metastasis and prognosis of patients with colorectal cancer. J Cancer Res Clin Oncol. 2004; 130:521–6. [PubMed: 15133662]
33. Jin S, Wang K, Xu K, Xu J, Sun J, Chu Z, et al. Oncogenic function and prognostic significance of protein tyrosine phosphatase PRL-1 in hepatocellular carcinoma. Oncotarget. 2014; 5:3685–96. [PubMed: 25003523]

34. Ren T, Jiang B, Xing X, Dong B, Peng L, Meng L, et al. Prognostic significance of phosphatase of regenerating liver-3 expression in ovarian cancer. Pathol Oncol Res. 2009; 15:555–60. [PubMed: 19247814]
35. Wang Q, Holmes DI, Powell SM, Lu QL, Waxman J. Analysis of stromal-epithelial interactions in prostate cancer identifies PTPCAAX2 as a potential oncogene. Cancer Lett. 2002; 175:63–9. [PubMed: 11734337]
36. Miskad UA, Semba S, Kato H, Yokozaki H. Expression of PRL-3 phosphatase in human gastric carcinomas: close correlation with invasion and metastasis. Pathobiology. 2004; 71:176–84. [PubMed: 15263806]
37. Li ZR, Wang Z, Zhu BH, He YL, Peng JS, Cai SR, et al. Association of tyrosine PRL-3 phosphatase protein expression with peritoneal metastasis of gastric carcinoma and prognosis. Surg Today. 2007; 37:646–51. [PubMed: 17643206]
38. Radke I, Gotte M, Kersting C, Mattsson B, Kiesel L, Wulfing P. Expression and prognostic impact of the protein tyrosine phosphatases PRL-1, PRL-2, and PRL-3 in breast cancer. Br J Cancer. 2006; 95:347–54. [PubMed: 16832410]
39. Fang XY, Song R, Chen W, Yang YY, Gu YH, Shu YQ, et al. PRL-3 Promotes the Malignant Progression of Melanoma via Triggering Dephosphorylation and Cytoplasmic Localization of NHERF1. J Invest Dermatol. 2015; 135:2273–82. [PubMed: 25897829]
40. Fagerli UM, Holt RU, Holien T, Vaatsveen TK, Zhan F, Egeberg KW, et al. Overexpression and involvement in migration by the metastasis-associated phosphatase PRL-3 in human myeloma cells. Blood. 2008; 111:806–15. [PubMed: 17934070]
41. Yagi T, Morimoto A, Eguchi M, Hibi S, Sako M, Ishii E, et al. Identification of a gene expression signature associated with pediatric AML prognosis. Blood. 2003; 102:1849–56. [PubMed: 12738660]
42. Park JE, Yuen HF, Zhou JB, Al-Aidaroos AQ, Guo K, Valk PJ, et al. Oncogenic roles of PRL-3 in FLT3-ITD induced acute myeloid leukaemia. EMBO Mol Med. 2013; 5:1351–66. [PubMed: 23929599]
43. Jeong DG, Kim SJ, Kim JH, Son JH, Park MR, Lim SM, et al. Trimeric structure of PRL-1 phosphatase reveals an active enzyme conformation and regulation mechanisms. J Mol Biol. 2005; 345:401–13. [PubMed: 15571731]
44. Sun JP, Wang WQ, Yang H, Liu S, Liang F, Fedorov AA, et al. Structure and biochemical properties of PRL-1, a phosphatase implicated in cell growth, differentiation, and tumor invasion. Biochemistry. 2005; 44:12009–21. [PubMed: 16142898]
45. Irwin JJ, Shoichet BK. ZINC--a free database of commercially available compounds for virtual screening. J Chem Inf Model. 2005; 45:177–82. [PubMed: 15667143]
46. Lang PT, Brozell SR, Mukherjee S, Pettersen EF, Meng EC, Thomas V, et al. DOCK 6: combining techniques to model RNA-small molecule complexes. Rna. 2009; 15:1219–30. [PubMed: 19369428]
47. Huey R, Morris GM, Olson AJ, Goodsell DS. A semiempirical free energy force field with charge-based desolvation. J Comput Chem. 2007; 28:1145–52. [PubMed: 17274016]
48. Shin G, Kang TW, Yang S, Baek SJ, Jeong YS, Kim SY, et al. GENT: gene expression database of normal and tumor tissues. Cancer Inform. 2011; 10:149–57. [PubMed: 21695066]

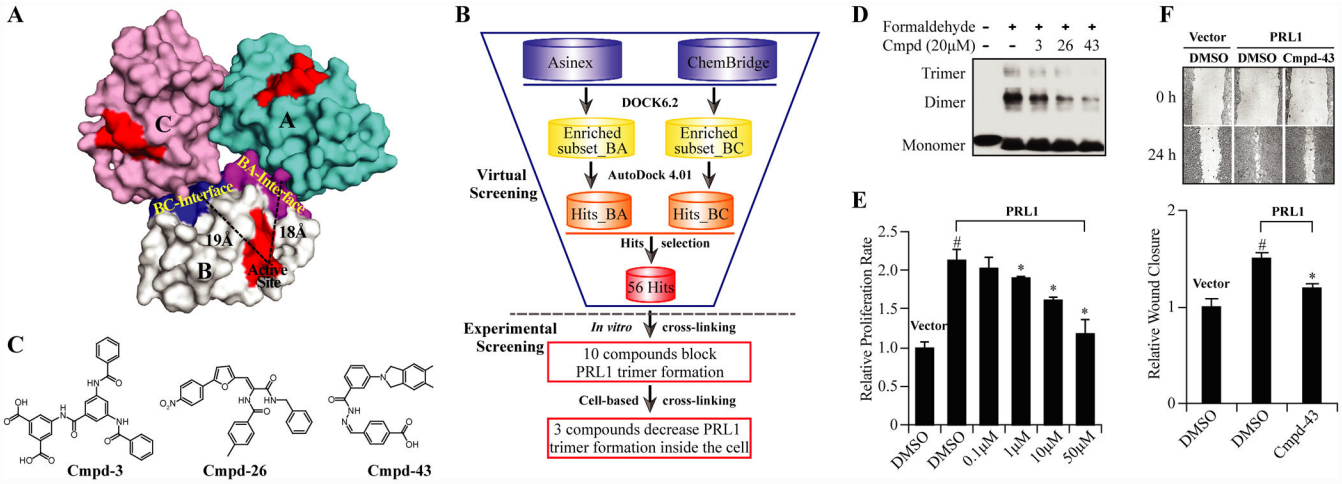

Figure 1. Identification of small molecules disrupting PRL1 trimerization

A. The representation of PRL1 trimer arrangement and the two interfaces, namely BA (purple, residues K125, Y126, E127, D128, V130, Q131, F132, R134, Q135, K136, R138, G139, L146, and E150) and BC (blue, residues E11, V12, T13, Y14, K15, N16, M17, R18, E36, K39, Y40, G41, F92, R93, P96, G97, C98, K136, and F160) interface within monomer B, which were defined as two separate docking sites in the virtual screening. The active site pocket is highlighted in red (residues C^{104}VAGLGR^{110}), and the distances between each dimer interface and the catalytic Cys104 are indicated by dash lines. **B**. The overall strategy to identify PRL1 trimer disruptor. **C.** Chemical structures of the top three hits from cross-linking assay. **D**. Effect of compounds 3, 26 and 43 on PRL1 trimerization inside the cells. **E**. Cmpd-43 inhibited PRL1 mediated cell proliferation. **F**. Cmpd-43 (10 μM) delayed the wound closure induced by PRL1 overexpression in HEK293 cells. Upper panel: representative microscopic images at different time (magnification, x100). Lower panel: quantification of the wound healing assay by measuring the relative wound closure. #p<0.05 (Student's t test) compared with control group; *p<0.05 (Student's t test) compared with PRL1 overexpressing HEK293 cells. Data represent mean (SD) of 3 independent experiments.

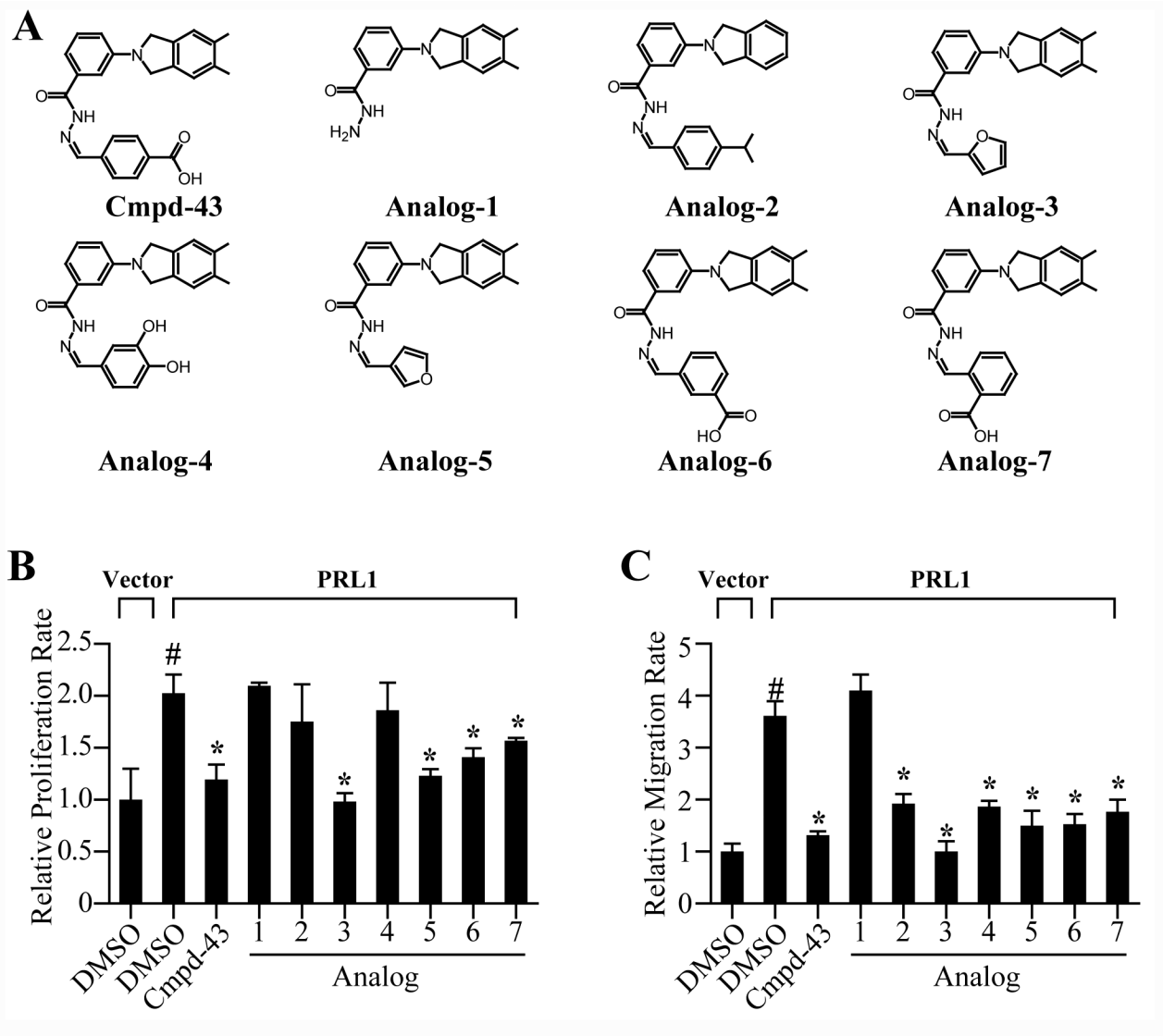

Figure 2. Structure and activity analysis of Cmpd-43 and its analogs

A. Chemical structures of Cmpd-43 and its analogs. **B**. The relative proliferation rate of PRL1 overexpressing cells treated with 10 μM of Cmpd-43 and its analogs. **C**. The relative migration rate of PRL1 overexpressing cells pretreated with 10 μM of Cmpd-43 and its analogs. #p<0.05 (Student's t test) compared with the control group; *p<0.05 (Student's t test) compared with PRL1 overexpressing HEK293 cells. Data represent mean (SD) value from 3 independent experiments.

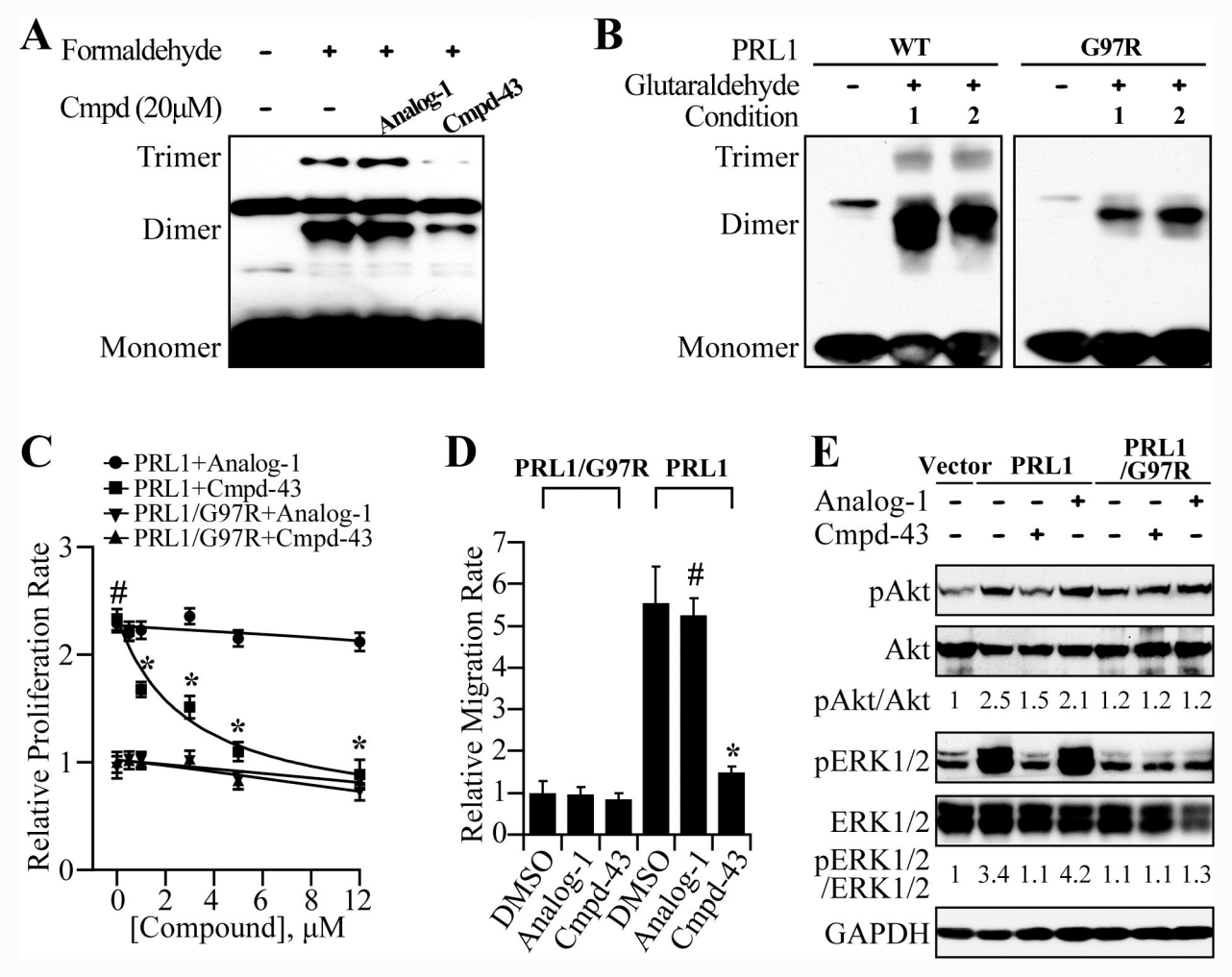

Figure 3. Specific inhibition of PRL1-mediated signaling, cell proliferation and migration by Cmpd-43

A. Cmpd-43, but not its inactive Analog-1, blocked PRL1 trimerization in HEK293 cells. **B**. PRL1/G97R has impaired trimer formation compared to wild-type PRL1. *In vitro* cross-linking assay was performed by incubating recombinant PRL1 or PRL1/G97R with 0.005% glutaraldehyde for either 10 min at RT (Condition 1) or 30 min on ice (Condition 2). **C**. Cmpd-43 specifically and dose-dependently suppressed the cell viability of wild-type PRL1 overexpressing HEK293 cells. **D**. Cmpd-43 (10 μM) specifically inhibited the migration of wild-type PRL1 overexpressing HEK293 cells. **E**. Cmpd-43 (5 μM) specifically inhibited PRL1 mediated ERK1/2 and Akt activation in HEK293 cells. #$p<0.05$ (Student's *t* test) compared with control group; *$p<0.05$ (Student's *t* test) compared with PRL1 overexpressing HEK293 cells. Data represent mean (SD) value from 3 independent experiments.

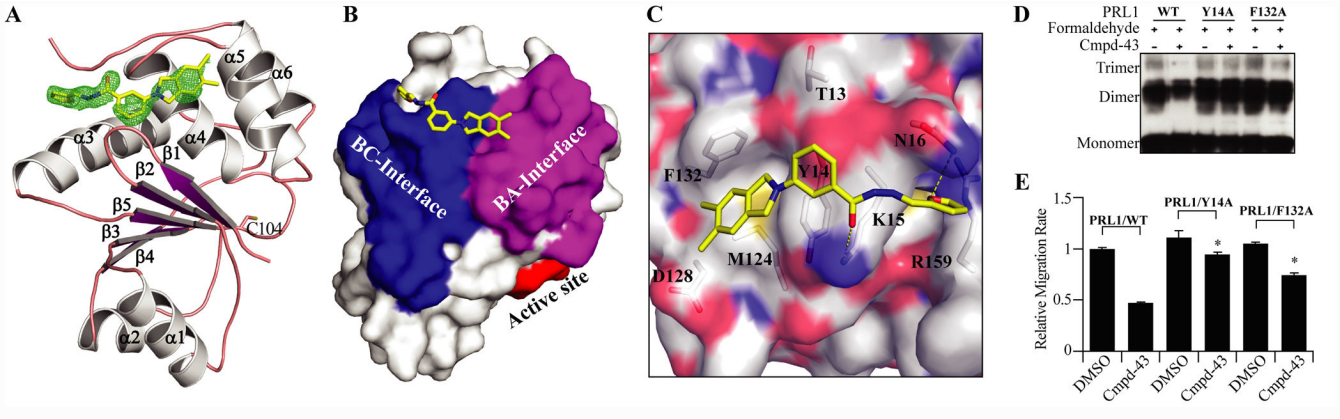

Figure 4. Analog-3 and Cmpd-43 bind to the PRL1 trimer interfaces and block PRL1 trimerization

A. The overall structure of PRL1•Analog-3. The PRL1 is shown in ribbon with secondary structure labeled. Analog-3 and the catalytic Cys104 are shown in stick. Unbiased *F*o-*F*c omit map of Analog-3 contoured at +2.5s is shown in green mesh. **B.** Analog-3 binds to an area at the backside of PRL1 active site, with the majority contact area in BC-interface and the minority in BA-interface. **C.** The close-view of Analog-3 binding with PRL1. Analog-3 and the residues within 5 Å distance of Analog-3 are shown in stick, with carbon atom colored in yellow and gray respectively. Two polar interactions are indicated by yellow dash lines. **D.** Effect of 20 μM Cmpd-43 on PRL1/Y14A and PRL1/F132A trimerization by *in vitro* cross-linking assay. **E.** The relative migration rate of PRL1/Y14A and PRL1/F132A in the presence of 10 μM Cmpd-43. **p*<0.05 (Student's *t* test) compared with wild-type PRL1 with Cmpd-43 treatment group. Data represent mean (SD) value of 3 independent experiments.

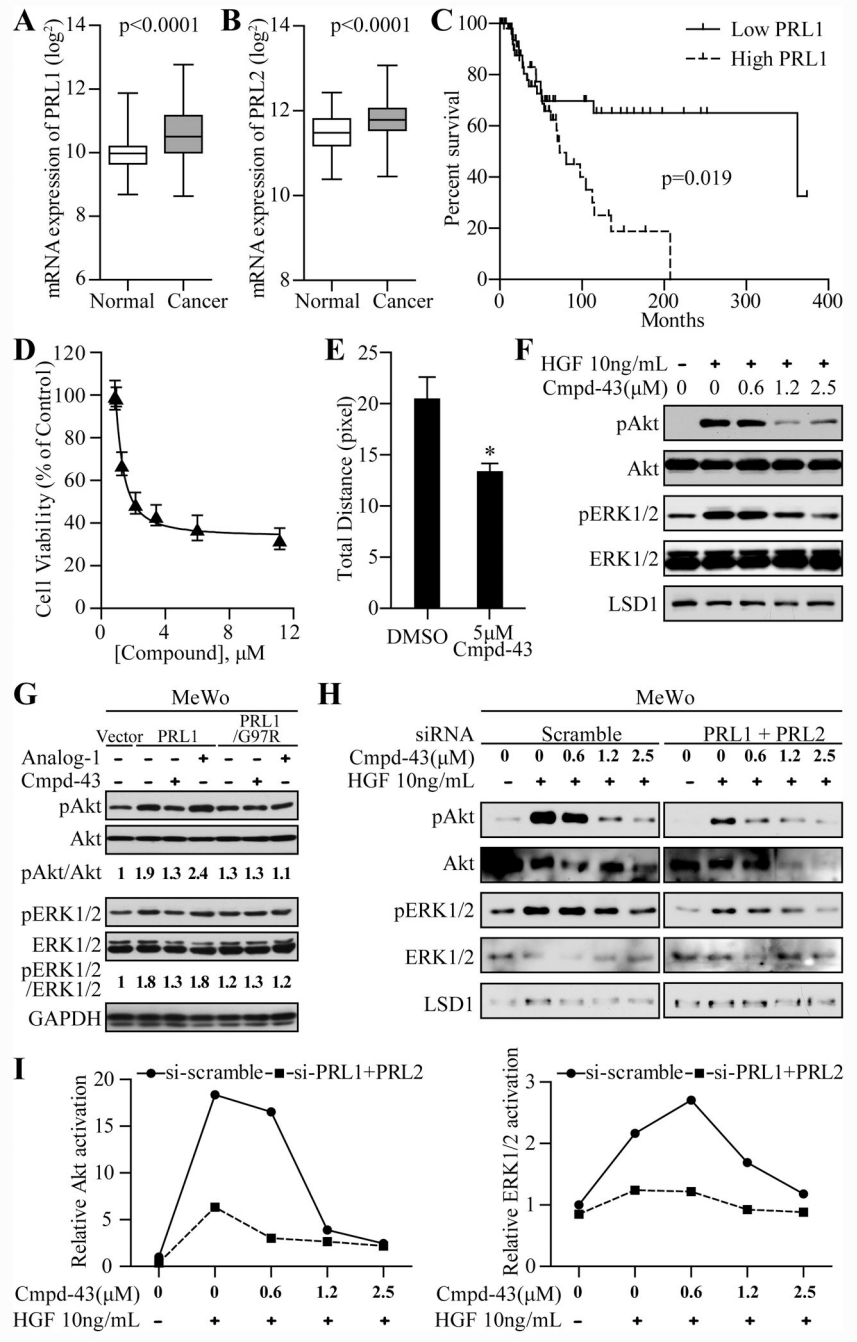

Figure 5. Cmpd-43 exhibits anti-cancer activity towards melanoma cell line MeWo

A and B. Differential expression of PRL1 (**A**) or PRL2 (**B**) mRNA between normal skin samples (n=141) and melanoma patient samples (n=302). **C.** Kaplan-Meier survival analysis of 110 melanoma patients, grouped by their status of PRL1 mRNA expression level. **D.** Cmpd-43 does-dependently suppressed MeWo cell proliferation. **E.** Cmpd-43 significantly reduced MeWo cell motility. Total distance is the average of full track length of more than 600 cells over 6 h. **F.** Cmpd-43 dose-dependently inhibited the HGF-induced ERK1/2 and Akt activation in MeWo cells. **G.** Cmpd-43 (2.5 μM) suppressed PRL1-overexpression

induced ERK1/2 and Akt activation. **H.** The inhibitory effect of Cmpd-43 towards HGF-induced ERK1/2 and Akt activation was significantly compromised in MeWo cells treated with siRNAs for both PRL1 and PRL2. **I.** The quantification of ERK1/2 and Akt activation in MeWo cells treated with either scramble siRNA or siRNAs for both PRL1 and PRL2. *$p<0.05$ (Student's *t* test) compared with DMSO control group. Data are representative of three independent experiments (mean and SD).

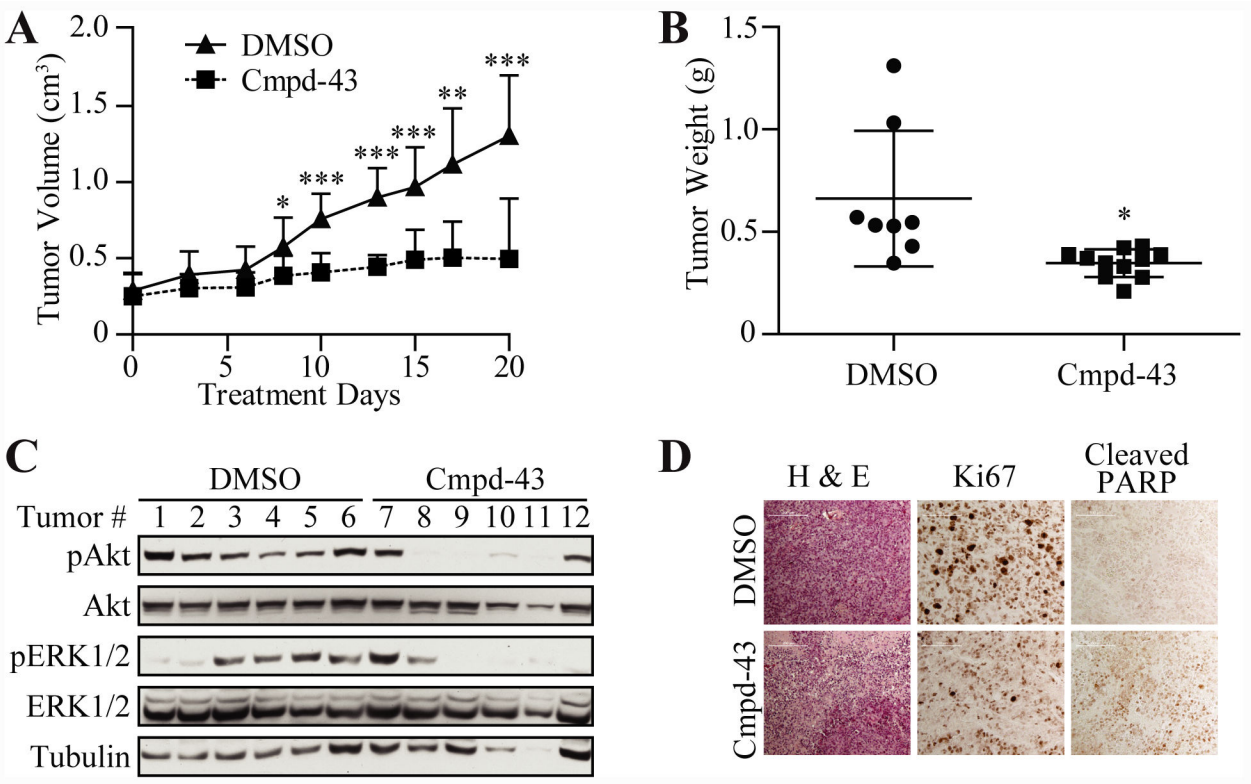

Figure 6. Cmpd-43 suppresses melanoma xenograft growth *in vivo*

A. The tumor volume of MeWo xenograft treated with either vehicle control or Cmpd-43 for 21 days. **B.** The final tumor weight of MeWo xenograft at 21 days. **C**. Cmpd-43 treatment inhibited both ERK1/2 and Akt activation in MeWo xenograft tumors. Numbers from 1 to12 indicate different tumor samples either from DMSO group (1-6) or Cmpd-43 treatment group (7-12). **D**. Cmpd-43 treatment significantly reduced proliferation and enhanced apoptosis in MeWo xenograft tumors. *p<0.05 (Student's t test) and *** p<0.001 (Student's t test) compared with control group.

Table 1
Data collection and refinement statistics

Crystal parameters	**PRL1•Analog-3**
Space group	$C222_1$
Cell Dimensions	
a (Å)	47.07
b (Å)	76.47
c (Å)	86.87
Data Collection	
resolution range (Å)	50.0 – 1.84
no. of unique reflections	13768
completeness (%)	98.0
redundancy	5.7
R_{merge} [a]	0.113
Refinement	
resolution range (Å)	50.0 – 1.90
no. of reflections used	11091
completeness (%)	87.2
no. of protein atoms	1230
no. of inhibitors	1
no. of ions	2
no. of waters	102
R_{work} [b]/R_{free} [c]	19.48/23.94
RMSD bond length (Å)	0.007
RMSD bond angle (°)	1.23

[a] $R_{merge} = \Sigma_h\Sigma_i|I(h)_i - \langle I(h)\rangle|/\Sigma_h\Sigma_i I(h)_i$.

[b] $R_{work} = \Sigma_h|F(h)_{calcd} - F(h)_{obsd}|/\Sigma_h F(h)_{obsd}$, where $F(h)_{calcd}$ and $F(h)_{obsd}$ were the refined calculated and observed structure factors, respectively.

[c] R_{free} was calculated for a randomly selected 3.6% of the reflections that was omitted from refinement.